An evaluation of membrane properties and process characteristics of a scaled-up pressure retarded osmosis (PRO) process

Wei He[1], Yang Wang[1], Iqbal M Mujtaba[2], and Mohammad Hasan Shaheed[1]

[1]*School of Engineering and Materials Science, Queen Mary, University of London, London E1 4NS, UK*

[2]*School of Engineering, University of Bradford, Bradford, BD7 1DP, UK*

E-mail: w.he@qmul.ac.uk, yang.wang@qmul.ac.uk, I.M.Mujtaba@Bradford.ac.uk, m.h.shaheed@qmul.ac.uk

Abstract:

This work presents a systematic evaluation of the membrane and process characteristics of a scaled-up pressure retarded osmosis (PRO). In order to meet pre-defined membrane economic viability (≥ 5 W/m^2), different operating conditions and design parameters are studied with respect to the increase of the process scale, including the initial flow rates of the draw and feed solution, operating pressure, membrane permeability-selectivity, structural parameter, and the efficiency of the high-pressure pump (HP), energy recovery device (ERD) and hydro-turbine (HT). The numerical results indicate that the performance of the scaled-up PRO process is significantly dependent on the dimensionless flow rate. Furthermore, with the increase of the specific membrane scale, the accumulated solute leakage becomes important. The membrane to achieve the optimal performance moves to the low permeability in order to mitigate the reverse solute permeation. Additionally, the counter-current flow scheme is capable to increase the process performance with a higher permeable and less selectable membrane compared to the co-current flow scheme. Finally, the inefficiencies of the process components move the optimal APD occurring at a higher dimensionless flow rate to reduce the energy losses in the pressurization and at a higher specific membrane scale to increase energy generation.

Keywords: pressure retarded osmosis, scaled-up, membrane sensitivity analysis, process characteristics, operating conditions.

* Corresponding author: Tel: + 44 (0)20 7882 33319
E-mail address: m.h.shaheed@qmul.ac.uk

1. Introduction

Renewable energy sources are increasingly becoming popular due to the shortage of the fossil fuels and the concerns of the global warming. In recent decades, renewable technologies, such as solar, wind, tidal, wave, biomass and energy storage devices, have been significantly investigated and are being applied widely in both industrial and private applications [1, 2]. However, due to the inherent intermittence of the most renewable energy sources, the stability and robustness in the case of energy generation from renewable energy sources need to be addressed [3, 4]. Osmotic energy, or salinity energy, released from the mixing of the salinity gradients (such as freshwater, river water and seawater) is also a source of renewable energy that is eco-friendly with no significant emission of greenhouse gases. In addition, compared to other renewable energy sources, it is less periodic and has no significant operational hazards. Pressure retarded osmosis (PRO) is one of the most developed technologies for osmotic energy extraction, which is reported achieving both higher efficiencies and higher power densities than the reverse electro-dialysis [5]. PRO is an osmotic driven membrane process. In PRO, water from an unpressurized low concentration side is transferred to a pressurized high concentration side due to the osmotic pressure difference between the membrane surfaces. Then, the permeation flows into a hydro-turbine and is expanded to generate electricity. PRO was invented by Sidney Loeb in 1970s' [6], and developed rapidly in recent years due to significant improvement of membrane performance [7] and innovative design [8]. In 2009, Statkraft, a Norwegian state-owned power company, opened the first PRO process and started to test the novel technology in real life [9]. However, in order to make PRO commercially attractive, the power density achieved was estimated to be at least 5 W/m^2 [10].

Previous studies mainly focused on the development of the high performance membrane and the evaluation on the lab-scale PRO process. In a lab-scale PRO process, as the limited membrane area utilised, the performance is actually the maximum or peak power densities. With a scaled-up process, the strengthened draw dilution and feed concentration accompanying with the water and solute transfer are inevitable and the realistic process performance would be totally different. Due to significantly improved membrane performance, the realistic PRO salinity power generation has become a hot topic in the field. But the accumulated detrimental effects during the mass transfer across the membrane substantially restrict the overall salinity energy generation. These detrimental effects commonly exist in osmotic-driven membrane process, including the internal concentration polarization (ICP) inside the support layer, external concentration polarization (ECP) on the draw solution side near the membrane surface, and the reverse solute permeation (RSP) across the membrane from the draw to the feed. A systematic study on these performance limiting effects of a lab-scale PRO have been carried out by Yip et al. [11]. The flux models of the water and solute considering all the ICP, ECP and RSP were derived and verified with the experimental results of different membrane properties [12]. Therefore, numerical modelling of the scaled-up PRO process can be developed on the basis of these transport equations to study the design and operation [13].

In fact, model development and numerical modelling of the scaled-up PRO process considering the ICP, ECP and RSP effects along the membrane channel and the spatial distribution of the concentration and flow rate have been investigated by several research groups worldwide. From the membrane module-level, a thermodynamic model of PRO is proposed [14] and the thermodynamic limits of the PRO process was identified by evaluating the extractable energy in reversible operation and constant-pressure operation [15]. A further model considering the effects of ICP, ECP and RSP is proposed and studied by Straub et al [16]. In addition to the model of the module-scale PRO,

inspired by the theory and design of the heat exchangers, Banchik et al. [17] and Sharqawy et al. [18] studied the reverse osmosis (RO) and PRO process as the membrane mass exchangers and derived systematic effectiveness-mass transfer units (ε-MTU) models for the future design in practice [17, 18]. They also investigated the overall membrane performance and identified the optimum operations of a PRO process based on ε-MTU model considering the CP effect [19]. Naguib et al. developed two procedures for modelling PRO including bench-scale membrane samples and commercial scale processes [20]. According to the simulation of the two selected commercial length membranes, average power densities were 4.6 and 5.6 W/m^2 [20]. In our previous study, a modelling framework of scaled-up PRO considering these detrimental effects is developed [21].

Based on these models, different configurations and operations of the scaled-up PRO are studied. In these investigations it is manifested that, due to the benefiting advantages of RO and PRO, hybrid RO-PRO system has become a hot topic. Kim et al. evaluated and compared four configurations of RO-PRO systems by numerical modelling considering the spatial distribution of concentration and velocity based on mass balance principle [22]. A PRO pilot system was studied by simulation and experiment in a hybrid RO-PRO process [23, 24]. According to the model-based simulation, it is estimated that the maximum power density of PRO can be approximately achieved up to 10 W/m^2 in the hybrid system by using virtual membrane [23]. While in the pilot system, average experimental power densities for the RO-PRO process ranged from 1.1 to 2.3 W/m^2 [24]. Recently, a novel solar PV assisted hybrid RO-PRO desalination plant is investigated and the simulations indicated the increased detrimental effects in PRO at the low fraction of the solar PV energy [25]. After all, development and validation of mathematical models of the scaled-up PRO process have been widely investigated. However, all the prior numerical investigations are mainly focused on the developing modelling framework of the evaluation of the detrimental effects in a scaled-up PRO. In these works, only one or two selected membranes are investigated by simulation to address the non-ideal effects coupled with the increased process scale. There is lack of the studies to investigate the integrated effect of the membrane permeability-selectivity with increased process scale and the operating conditions.

In fact, the challenge in a scaled-up PRO process is the decreased average power density with the increase of the process scale [26]. According to the analysis carried out by Statkraft [10], the satisfactory power density should be no less than 5 W/m^2 to achieve economic viability. Due to inherent trade-off challenge between power density and specific energy in a full-scale PRO process [16], optimizing the process configuration, membrane properties, operating conditions and components efficiency including high-pressure pump (HP), energy recovery device (ERD) and hydro-turbine (HT) are crucial to balance these two objectives and to improve the performance of PRO process. For accelerating the implementation of PRO process, therefore, the process dynamics and the influential factors of the scaled-up PRO process need to be investigated and figured out. Moreover, membrane is the core component in the PRO process and its performance determines the overall economic and energy performance of the system. Several investigations focusing on the membrane fabrication reported the existence of permeability-selectivity trade-off relationship. These studies also addressed the optimum membrane properties and the resulting maximum peak power densities by developing sensitivity analysis of membrane properties in a lab-scale PRO [11]. Furthermore, in a scaled-up PRO, the existing trade-off relationship of the membrane permeability and rejection is coupled with the spatial variations of the flow, heat and mass transfer, the problem becomes complicated. In order to improve the particular membrane properties for a scaled-up PRO,

a balanced membrane performance needs to be identified considering different operating conditions and the increase of the process scale. However, there is no reported published work on the membrane sensitivity analysis on the scaled-up PRO performance with respect to different operating conditions. Only a particular membrane with a selected set of membrane water permeability coefficients, solute permeability coefficients and structural parameters was selected for studying the module-scale or scaled-up PRO process in previous studies [13, 15-19, 21, 23]. Therefore, in this study, a sensitivity analysis of the membrane properties aims to be developed in a scaled-up PRO to investigate the optimum properties in different operating conditions, such as different flow schemes (co-current and counter-current flow scheme) and flow fractions of the salinities. Additionally, at a system-level, energy losses in energy generation, water pumping and pressurisation significantly affect the overall performance of the scaled-up PRO. Therefore, in this study, the effects of the inefficiencies of the components (HP, ERD and HT) are also addressed in this study.

2. Mass transfer in pressure retarded osmosis

2.1. Pressure retarded osmosis and two basic flow schemes

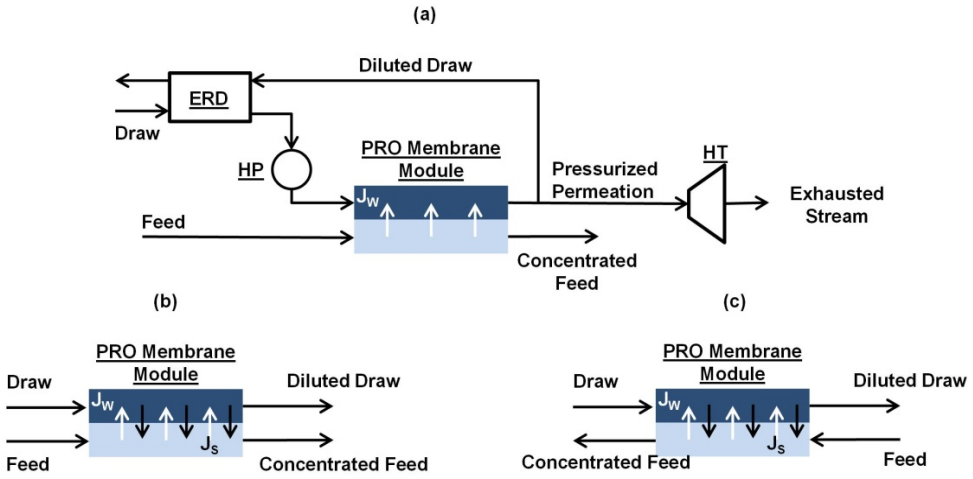

Figure 1 Schematic diagram of a classic PRO process in (a). Two simple flow schemes of the process, the co-current flow scheme and the counter-current flow scheme, are shown in (b) and (c), respectively.

PRO uses the natural phenomenon of osmosis to permeate water across a semi-permeable membrane from a side with low solute concentration and low hydraulic pressure to a side with high concentration and high pressure. A classic PRO process is illustrated in Fig. 1(a) in which a HP, an ERD, a PRO membrane module, and a HT are included. In this study, the scale of the PRO membrane module refers to the membrane area used in the module. The permeated water is transferred from the feed side to the draw side due to the non-zero osmotic driving force. In a classical PRO process, partial of the diluted draw solution from the outlets is used to pressurize the initial draw solution in the ERD, and the pressurized permeation (remaining diluted draw solution) is expanded in the HT to generate electricity. As water is transported across the membrane, the draw solution becomes progressively diluted and the feed solution becomes concentrated.

Simple co-current and the counter-current flow configurations are illustrated in Fig. 1(b) and 1(c), respectively. In a co-current PRO process, both the draw and feed solution flow in the same direction (from the left to the right as illustrated in Figure 1(b)). Flowing in the same direction of the flow

along each flow channel, the concentrations of the draw solution and the feed solution are changing. Conversely, in a counter-current PRO process, the draw and the feed solution flow in the opposite directions (from the left to the right for the draw solution and from the right to the left for the feed solution as illustrated in Fig. 1(c)).

2.2. Mathematical model

In a PRO process, the membrane power density is determined by the trans-membrane hydraulic pressure difference and the water permeation flux across the membrane [10] represented as,

$$W = J_W \cdot \Delta P_{PRO} \tag{1}$$

where J_W is the water flux across the membrane. It can be expressed as

$$J_W = A(\Delta\pi_m - \Delta P_{PRO}) \tag{2}$$

where A is the membrane permeability coefficient, $\Delta\pi_m$ and ΔP_{PRO} are the osmotic pressure difference and hydraulic pressure difference between the two sides of the membrane surface. Due to negligible pressure drop along the flow channel, constant hydraulic pressure difference is considered within the membrane module. The osmotic pressure of a dilute solution can be estimated by using the van't Hoff's law. In this study, with the modified van't Hoff coefficient [17, 18], the osmotic pressure difference can be represented as,

$$\Delta\pi_m = C_{OS}(c_{D,m} - c_{F,m}) \tag{3}$$

where C_{OS} is the modified van't Hoff coefficient from [17, 18], $c_{D,m}$ and $c_{F,m}$ are the concentration of the draw and feed solution near the membrane surface in the draw and feed channel, respectively.

In an ideal PRO process, at the steady-state operation, the concentration of the salinity in each solution is distributed homogenously that there is no difference of the concentration between the bulks and the flows near the surface of the membrane. However, during the mass exchange process in a PRO process, with the current membrane performance, the ICP, ECP and RSP effects are not negligible. Due to the existence of these performance limiting effects, the real net driving force of the water transportation is lower than the net driving forces estimated in terms of the bulks. Yip et al. developed a systematic investigation of all the performance limiting phenomena on water flux and power density of PRO process [11]. According to Yip et al.'s work, considering the ICP, ECP and RSP, concentration difference between the two sides of the membrane can be represented as

$$c_{D,m} - c_{F,m} = \frac{c_D \exp(-J_W / k) - c_F \exp(J_W S / D)}{1 + \frac{B}{J_W}[\exp(J_W S / D) - \exp(-J_W / k)]} \tag{4}$$

where c_D and c_F are concentrations of the bulk draw and the bulk feed, respectively. B is the membrane solute permeability coefficient, D is the bulk diffusion coefficient, $k = D/\delta$ is the boundary layer mass transfer coefficient in which δ boundary layer thickness, and $S = t_s\tau/\varepsilon$ is the

support layer structural parameter in which t_s is the thickness of the porous layer, τ and ε are the tortuosity and porosity of the support layer of the membrane respectively.

On the basis of the concentration difference across the membrane surfaces, the water flux and the reverse solute permeation flux can be obtained. The water flux considering the ICP, ECP and RSP effects can be expressed as

$$J_W = A(C_{os}(\frac{c_D \exp(-J_W / k) - c_F \exp(J_W S / D)}{1 + \frac{B}{J_W}(\exp(J_W S / D) - \exp(-J_W / k))}) - \Delta P_{PRO}); \quad (5)$$

In addition, different from the water flux, the reverse solute flux is only dependent on the concentration difference. It can be represented as

$$J_S = B(c_{D,m} - \mathrm{c}_{F,m}) = \mathrm{B}(\frac{c_D \exp(-J_W / k) - c_{\mathrm{F}} \exp(J_W S / D)}{1 + \frac{B}{J_W}(\exp(J_W S / D) - \exp(-J_W / k))}) \quad (6)$$

Both the water flux and reverse solute permeation flux are the local mass transfer rates. The overall performance of the entire membrane usage can be obtained by integrating the fluxes along the membrane usage. The water flux across the membrane is, in fact, the velocity of the permeated mass flow per unit area of membrane. From this viewpoint, at the steady state, the water flux of the full scale PRO membrane can be expressed as,

$$d(\Delta V_P) = J_w d(A_m); \quad \Delta q_P = \rho_P \Delta V_P \quad (7)$$

where ΔV_P is the permeated flow rate of water, and A_m is the area of the membrane. Δq_P is the mass flow rate of the permeation and ρ_P is the density of the permeation which is changing along the membrane channel depending on the local hydrodynamics and membrane condition. Therefore, at a particular position, the water permeates from the feed side to the draw side due to the non-zero net driving force. The flow rate of the local permeation (both volumetric and mass flow rates) can be estimated based on the local condition of the solution and membrane. In addition, when RSP effect is included in the modelling, the transportation rate of the reverse solute permeation is also crucial and can be expressed as

$$d(\Delta V_S) = J_S d(A_m); \qquad \Delta m_S = \rho_S \Delta V_S \quad (8)$$

where ΔV_S and Δm_S are the volumetric flow rate and mass flow rate of the reverse solute flow, respectively. ρ_S is the density of the reverse solute flow. Similar to density of permeation, density of reverse solute flow is also a local variable which is changing along the flow channel.

The flow rates in the both the draw and feed solution and concentration, are assumed to be only varied along the membrane channel from the inlet to the outlet. It indicates that the flow can be considered as a one dimensional flow problem for each channel. Therefore, based on the mass balance, the concentration and flow rate of the draw solution and the feed solution in the channels can be presented as

$$c_D = \frac{c_D^0 q_D^0 - \Delta m_S}{q_D^0 + \Delta q_P}; \quad q_D = q_D^0 + \Delta q_P$$
$$c_F = \frac{c_F^0 q_F^0 + \Delta m_S}{q_F^0 - \Delta q_P}; \quad q_F = q_F^0 - \Delta q_P \tag{9}$$

where the superscript 0 denotes the state of the concentration and flow rate at inlet. From the perspective of the process performance, the specific extractable energy (SEE) of a constant-pressure PRO process is

$$E_{C-PRO} = \frac{\Delta P_{PRO} \Delta V_P}{V_F^0} \tag{10}$$

The SEE is the energy extracted per flow rate of the initial feed solution. For a PRO process in coastal regions using natural salinity gradients to generate electricity, such as seawater and freshwater/river, compared to the enormous volume of the seawater, the available volume of the low concentration stream is always limited and thus needs to be utilized efficiently. Therefore, the SEE of a PRO process is, accordingly, defined and used as one of the objectives of this study.

Moreover, in order to evaluate the average membrane performance, another objective, average power density (APD), is defined as

$$e = \frac{E_{C-PRO} V_F^0}{A_M} \tag{11}$$

The details of the steady-state model and modelling framework of PRO can be found in our previous work [21]. Based on the models, the simulation of the two flow schemes was carried out with the following assumptions: i) a constant hydraulic pressure is applied on the draw solution, and no pressure is applied on the feed solution and pressure drop through the flow channel is negligible in the case of both feed and draw solutions of both the flow channels; ii) osmotic pressure is linearly proportional to the concentration difference based on the modified van't Hoff law [27]. In the salinity range of 0-70 g/kg, the modified linear osmotic pressure approximation is validated and the maximum deviation is found to be 6.8% [17, 18]; iii) mass flow rates are averaged over the cross-sectional area of the two flow channels. Accordingly, it becomes a one-dimensional problem in each flow channel, and the mass transfer coefficient is constant when the effect of ECP is considered; iv) membrane fouling and deformation is ignored. And the membrane water permeability coefficient, salt permeability coefficient and structure are assumed to be constant in different operating condition. v) From the previous studies, it is observed that the insignificant effect of density variation on the solutions obtained in the range of salinity studied [28, 29], for simplicity, a constant density of the water is used for both draw and feed solutions [30], which is 1,000 kg m^{-3}. The efficiency of the components in a PRO process, including HP, ERD and HT, are considered as 100% in section 3 and 4 and the influence of the inefficiency is investigated in section 5.

In this work, sensitivity analysis and process characteristics of PRO with respect to operating condition, membrane properties and components (HP, ERD and HT) are aimed to be studied. The analysis can be achieved through a series of simulations with different parameters. In each simulation, all the parameters are given and the process performance in terms of SEE and APD can be evaluated. The flowchart of the numerical work is illustrated in Fig. 2.

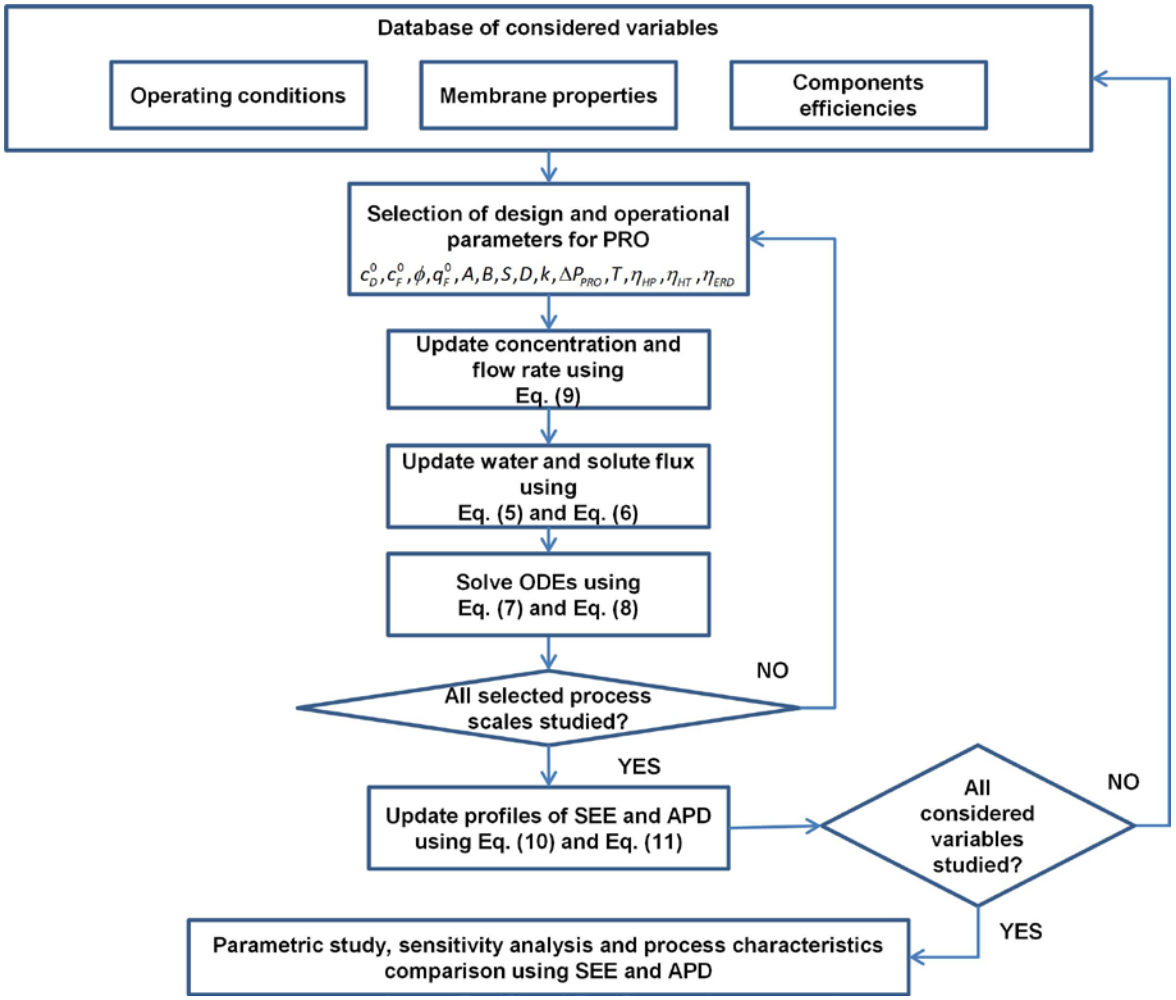

Fig. 2. Flowchart of the sensitivity analysis and process characteristics of PRO in this work.

A database of PRO process variables including operating conditions, membrane properties, and components efficiencies is identified first. For each case study, a particular combination of the variables is selected. In the simulation, with selected design parameters and operations in the simulations, the salt concentration of the draw and feed solution are updated by substituting water flux represented by equations (5) and reverse solute flux represented by equation (6) into permeated water mass flow rate expressed by equation (7) and accumulated solute permeation rate expressed by equation (8). A system of ordinary differential equations (ODEs) on mass rates of permeated water and reverse solute permeation can be obtained to describe the steady-state PRO process. Moreover, with the inlet and outlet conditions of the co-current and counter-current flow PRO discharge, the ODEs can be solved, and profiles of water flux and power density can be obtained with the increase on the process scale. Then, the SEE and the APD can be obtained by equation (10) and (11). After the evaluation of a particular PRO process performance, the next combination of the variables is selected for the simulation. If all the combinations of the pre-defined variables are studied, the simulation stops and all the results of the SEE and APD are used to be compared and analyzed to address the influences of operating operation, membrane properties and components efficiencies. The ODEs are implemented in MATLAB software and solved by the ode-solvers.

3. Influence of operating conditions on performance of the scaled-up PRO process

Generally, the parameters of salinities include concentration and mass flow rates of both the high and low concentration solutions. The available natural saline streams that are potential draw solution comprise seawater and brackish water. Conversely, the low concentration water, such as river, sewage, industrial wastewater and private effluent can be used as feed water. In addition, brackish water and seawater can be considered as the feed solution if the high concentrated brine is available. In order to reduce the propensity of the membrane fouling, the streams need to be pre-treated. In this study, relationship between the mass flow rates of the two solutions is described by dimensionless flow rate, ϕ, which is feed fraction and defined as the ratio of the initial mass flow rate of the feed solution to the sum of the initial mass flow rates of both feed and draw solutions which can be represented as

$$\phi = \frac{q_F^0}{q_F^0 + q_D^0} \tag{12}$$

where q_F^0 and q_D^0 are the initial flow rates of the draw and feed solution, respectively.

One of the important operating conditions is the hydraulic pressure applied on the draw solution. A constant hydraulic pressure difference is applied in the PRO process. For a full scale PRO discharge, the balance is established between the osmotic pressure difference and the hydraulic pressure difference at the outlet of the membrane module.

In this study, furthermore, a parametric study of applied pressure is developed in the scaled-up PRO process and a comparison of the influences of the hydraulic pressure on the SEE and the APD are carried out in both the co-current and the counter-current flow schemes. The results are shown in Fig. 3 in which the SEE are represented by colour-map and the APD are represented by contour-line. Three cases of the dimensionless flow rates, 0.2, 0.5 and 0.8, are selected for representing the low, medium and high dimensionless flow rates. The selection of these three ratios aims to represent different feed fractions of the possible salinity gradients. The scale of the membrane area is studied in terms of specific membrane area which is the membrane area per initial flow rate of the feed solution. The investigated specific membrane area is up to 0.4 m^2 per 1 $L \cdot h^{-1}$ feed solution which is sufficient for a full scale PRO discharge in different operations. The other parameters are listed in Table 1. Constant initial flow rate of the feed solution is considered in this study. Thus, the membrane area is proportional to the specific membrane area and can be obtained based on the initial flow rate of the feed solution and specific membrane area.

TABLE 1 Parameters used in simulation of the scaled-up PRO.

Parameters	Value
Concentration of the draw solution	35 g/kg
Concentration of the feed solution	0.1 g/kg
Mass transfer coefficient	138.6 L $m^{-2}h^{-1}$ [11]
Diffusion coefficient	1.49×10^{-9} m^2 s^{-1} [31]
Modified van't Hoff coefficient	0.7307 bar kg g^{-1} [18] at 298 K
Initial feed flow rate	1 $L \cdot h^{-1}$
Membrane permeability coefficient	1.74 L $m^{-2} \cdot h^{-1} bar^{-1}$ [11]

Membrane solute permeability coefficient	0.16 L $m^{-2} \cdot h^{-1}$ [11]
Membrane structural parameter	307 μm [11]

According to the results, at the same dimensionless flow rate, the trade-off relationship between the SEE and the APD can be found. When a large scale of the membrane is used, the SEE is found to be high while the APD is found to be low. Conversely, at a small specific membrane scale, the SEE is very low when the APD is high. It is the result of the vanishing net driving force of the permeation due to the dilution of the draw and the concentration of the feed during the PRO discharge. Thus, in order to increase the membrane efficiency and reduce the membrane cost, a high APD should be aimed to achieve with the loss in the SEE. In addition, comparing the SEE between the two schemes, it is easy to find the advantageous efficiency of the counter-current flow scheme in the energy extraction. On the basis of the colour-map of SEE, the SEE of the counter-current flow scheme is larger than that of the co-current flow scheme at a particular dimensionless flow rate, especially in a high specific membrane scale. In contrast, the differences of the APD between the two flow schemes are not obvious, especially in the range of high APD. Comparing the contour-line of APD 3 and 5 W/m^2, the range of the dimensionless flow rate and the membrane scale are quite similar. At the dimensionless flow rate 0.2, the range of the APD larger than $1W/m^2$ has a slightly wider validated specific membrane area in the counter-current PRO process. Therefore, from the perspective of the APD, there is no obvious difference between the co-current and the counter-current flow scheme in the range of high APD. Conversely, with the increase on the specific membrane scale, in the range of the low APD, enhanced performance of the APD can be achieved in the case of the counter-current flow scheme.

However, operating pressure and membrane usage in a PRO process are always concerned. A high pressure operation requires high performance membrane module with proper spacer, membrane property and design. And a large membrane usage significantly affects the capital investment and maintenance cost. Based on the map of SEE and APD shown in Fig. 3, as a result, the PRO process can be possibly operated at a lower pressure with less membrane scale to achieve the same APD if the loss of part of the SEE is acceptable. The appropriate operations can be selected along the contour lines of APD in the range of lower hydraulic pressures and smaller specific membrane area.

Moreover, according to the results shown in Fig. 3, the most important influential factor to determine the SEE and APD of a membrane module is the dimensionless flow rate. In Fig. 3, the most validated operations to achieve the economically viable APD (≥ 5 W/m^2) is largest in the process with a dimensionless flow rate 0.2. In contrast, in the case of dimensionless flow rate 0.8, there is the smallest range of the preferred operations whose APD is economically viable. And the maximum SEE is significantly large when the dimensionless flow rate is 0.2. Therefore, from the perspective of the salinity energy generation and the overall membrane performance in the membrane module, a low dimensionless flow rate is preferred.

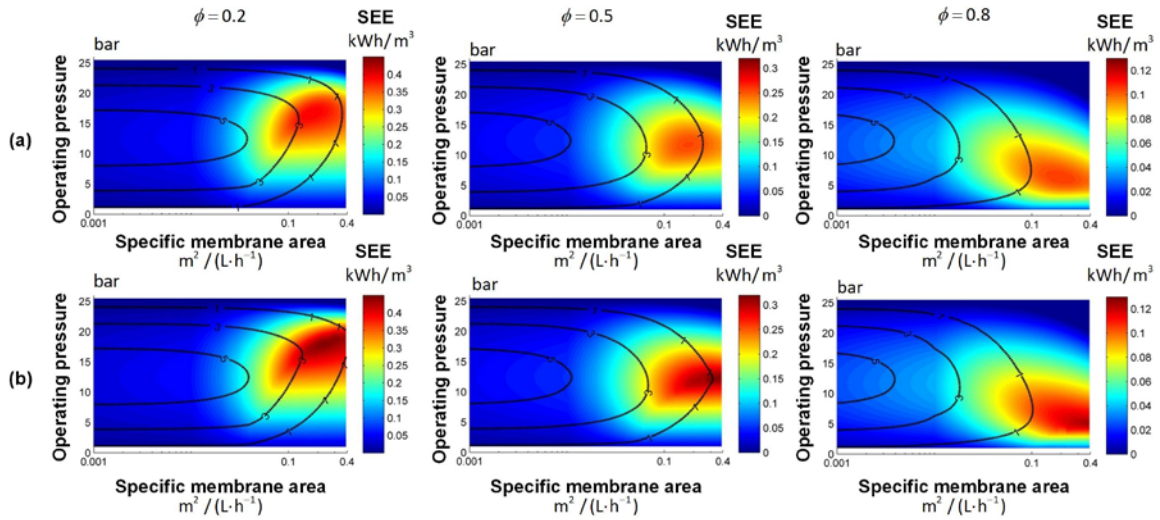

Fig.3. Influence of the applied hydraulic pressure on the performance of the scaled-up PRO process. The results of the co-current and the counter-current PRO processes are shown in row (a) and (b), respectively. Three dimensionless flow rates, 0.2, 0.5 and 0.8, are selected representing different conditions of the salinity gradients. The SEE are represented by colour-map and the APD are shown in contour-line.

4. Influence of membrane properties on the performance of scaled-up PRO process

At the heart of the membrane process, membrane performance is always one of the hottest topics in the field. The permeability-selectivity trade-off relationship commonly exists and governs the separation membranes [32-34]. Previous studies have demonstrated that the enhanced PRO membrane performance was attributed to the high water permeability of the active layer coupled with a moderate salt permeability and the ability of the support layer to suppress the leakage of the salt into the porous support layer [12]. Several detailed studies on the membrane properties and the influences on a coupon-scale PRO process can be found in the literature [11, 12, 31]. However, the sensitivity analysis of the membrane properties has not been studied in the case of a scaled-up PRO process. Therefore, in this section the performance of the scaled-up PRO process with different membranes is presented. First the identified trade-off membrane permeability and selectivity is introduced in Section 4.1. And a sensitivity analysis of the membrane properties is carried out in the scaled-up PRO process in Section 4.2.

4.1. Trade-off relationship between the water and solution permeability of PRO membrane

A systematic study to determine the permeability-selectivity trade-off relationship for the thin film composite (TFC) polyamide membranes can be found in [11]. According to their study, a trade-off relationship between the water and salt permeability coefficients of TFC polyamide membranes subject to chlorine-alkaline modification can be expressed as

$$B = \frac{L^{\beta}}{\lambda}\left(\frac{R_g T}{M_W}\right)^{\beta+1} A^{\beta+1} \tag{13}$$

where L is the thickness of the active layer, M_W is the molar mass of water, R_g is the gas constant, T is the absolute temperature, λ and β are the fitting empirical parameters. A set of the fitting parameters are obtained based on the data from publications on the hand-cast polyamide PRO membranes [11]. With this relationship between the permeability and selectivity of a TFC membrane,

a number of permeability-selectivity paired coefficients can be obtained. The fitting parameters used in this study are shown in Table 2. Other parameters include temperature 298 K, molar mass of water 18 g·mol^{-1}, and the gas constant 8.314 J·K^{-1}·mol^{-1}.

TABLE 2

Fitting parameters for the permeability-selectivity trade-off relationship of the TFC membrane [11].

Parameter	Value
β	2
λ	0.37×10^{-7} cm^4/s^2
L^{β}/λ	6.11×10^{-3} s^2/cm^2

4.2. Sensitivity analysis of membrane properties

On the basis of the permeability-selectivity trade-off of the TFC membrane properties, from recent literatures, membranes with satisfactory performance can be divided into low, medium and high permeable membrane according to the water permeability in the range of 1.42 – 7.76 L m^{-2}·h^{-1}bar^{-1} [11]. In addition, the range of the structural parameter, S, is also restricted by the types and functions of the membrane. The structural parameter usually ranges from 10-10,000 μm, including conventional TFC reverse osmosis membranes ($S = 10000$ μm) [12], hollow fibre membranes ($S = 600-1400$ μm) [35], hand-cast flat sheet membranes ($S = 300-3000$ μm) [36] and nano-fibre composite membranes ($S = 80-110$ μm) [37]. Therefore, membrane with water permeability coefficient in the range of 0 to 8 L m^{-2}·h^{-1}bar^{-1} and the structural parameter of 10-10000 μm are selected to represent the possible membrane properties. According to the trade-off relationship represented by equation (13), the corresponding membrane solute permeability coefficient is in the range of 0 to 6.29 L m^{-2}·h^{-1}. Thus, on the basis of the selected range of the permeability, selectivity and structural parameter of the membrane, the sensitivity analysis of membrane properties on the performance of the scaled-up PRO process can be carried out.

In order to achieve high APD of the membrane which is close to the economic viability, based on the results in section 3, three specific membrane scales, 0.01, 0.5 and 0.1 m^2/(L·h^{-1}), are selected. For simplicity, dimensionless flow rate 0.5 is selected and the results are shown in Fig. 4 in which both the co-current and the counter-current flow schemes are presented in row (a) and (b), respectively. The optimum properties of the membrane properties achieving the maximum SEE and APD at a particular structural parameter are presented by the dashed lines in all scaled-up PRO processes studied. According to the results, generally, the enhanced performance is attributed to the increased water permeability of the active layer coupled with a moderate salt permeability and the ability of the support layer to suppress the accumulation of the leakage salt. On the left of the dashed line, the increase on the membrane water permeability coefficient benefits the PRO process because it allows a higher volume of water permeation, and hence, the SEE increases to the maximum. In contrast, on the right of the dashed line, the salt leakage accumulated in the porous layer overwhelms any benefit from a higher water permeability membrane due to the inherent trade-off relationship.

Consequently, at a very small scale of the PRO process 0.01 $m^2/(L\cdot h^{-1})$, such as the coupon-scale or lab-scale PRO process, the dilution of the draw and the concentration of the feed are not significant. Thus, the SEE between the co-current and the counter-current process are similar to the investigated peak power densities with the different membrane properties in [11]. Furthermore, with the increase on the specific membrane scale, different level of influences of membrane properties on the scaled-up process performance is observed. In both the co-current and the counter-current flow PRO processes, with the increase of the specific membrane scale, the maximum SEE occurs at a lower membrane water permeability coefficient especially in the range of low structural parameter. For example, in the co-current PRO process as shown in row (a), the maximum SEE profile (dashed line) occurs at a lower membrane permeability coefficient with the low structural parameter. The optimum membrane permeability represented by the dashed line is nearly 8 L $m^{-2}\cdot h^{-1}bar^{-1}$ in PRO scale 0.01 $m^2/(L\cdot h^{-1})$, is nearly 4 L $m^{-2}\cdot h^{-1}bar^{-1}$ in PRO scale 0.05 $m^2/(L\cdot h^{-1})$, and is slightly higher than 2 L $m^{-2}\cdot h^{-1}bar^{-1}$ in PRO scale 0.1 $m^2/(L\cdot h^{-1})$ at the structural parameter 10 μm. Similar trend has been also found in the counter-current flow scheme. This indicates that with the different specific membrane scale of the PRO process, the balance of the trade-off between the permeability and selectivity to achieve the maximum SEE varies. The detrimental effect of the RSP plays a more significant role with the increase on the specific membrane scale. And thus, the increased specific membrane scale requires the preferred membrane properties to move to the higher selectivity of the membrane to mitigate the solute leakage and to achieve the maximum SEE extraction.

In addition, comparing the dependency of the membrane properties in the case of the two flow schemes, the membrane performance is also different. It is found that the maximum SEE profile occurs at slightly higher membrane permeability in the counter-current flow scheme. When the structural parameter is low, the preferred membrane permeability shifts to the high value obviously, as shown in Fig. 4. This means that the ability to increase the SEE by enhancing the membrane permeability is better for the counter-current flow scheme. A higher reverse solute permeability coefficient is acceptable for the counter-current PRO process to access a higher permeable membrane. As a result, the counter-current flow scheme performs better than the co-current flow scheme and more SEE and APD can be achieved in the counter-current flow schemes with the same salinity gradients using a higher permeable membrane.

Therefore, from the perspective of development and selection of the high performance membrane in a scaled-up PRO process, the requirements may be different from those for the maximum peak power densities. First, due to the accompanying increase in the solute leakage, high permeable membrane is not always the better choice for the energy extraction when the scale of the process increases. For a large scale PRO process, a medium or a low permeable membrane may be more efficient in order to reduce the accumulated solute leakage. Furthermore, different flow schemes of the PRO process are suited to different membranes for the maximum SEE extraction. Therefore, for a specific flow scheme, the selection of the membrane should be considered.

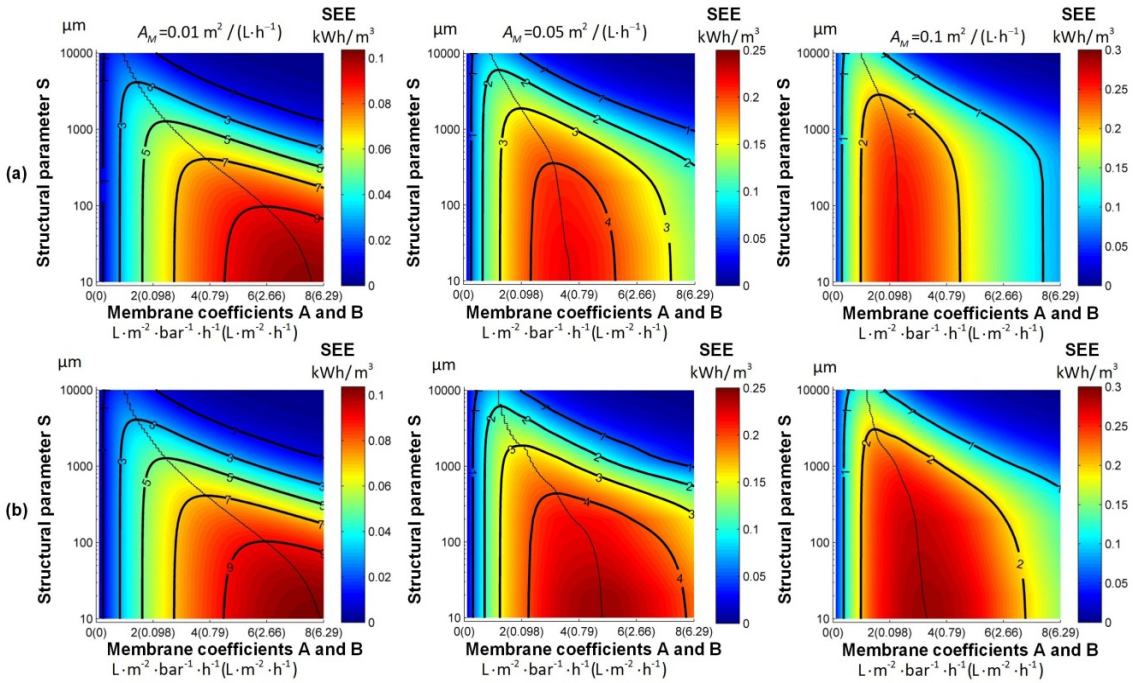

Fig. 4. Influence of membrane properties on the performance of the scaled-up PRO process. The results of the co-current and the counter-current PRO process are shown in row (a) and (b) respectively. Three membrane scales 0.01, 0.5 and 0.1 $m^2/(L{\cdot}h^{-1})$, are selected. The SEE are represented by colour-map and the APD are shown in contour-line. The dimensionless flow rate is 0.5. The membrane solute permeability coefficient is shown in bracket next to the membrane water permeability coefficient on the x-axis. A and B are defined in Equation (13)

Due to the accumulative reverse solute leakage, high permeable membrane may result in a poor performance in a scaled-up PRO process, according to the SEE and APD shown in Fig. 4. Moreover, there is no operation to meet the targeted economically viable APD (5 W/m^2) in specific membrane scale 0.05 and 0.1 $m^2/(L{\cdot}h^{-1})$. Does it mean the technology is difficult to scaled-up? Actually, equation (13) and the fitting parameters shown in Table 2 to describe the trade-off permeability-selectivity of membrane are empirical correlation and parameters. These empirical correlation and parameters are built up mainly based on membrane developed no later than 2011. Recently, with the rapid development of the high performance membrane, the trade-off permeability-selectivity of the membrane has been considerably improved. Several improved membranes are found from literatures and listed in Table 3. However, in order to meet the economic viability, how much improvement do we need? An analysis is presented in this section to find a solution.

TABLE 3 Several membranes from literatures in 2012 – 2015. B_{Eq} is membrane salt permeability coefficient based on equation (13).

Publications	A [L/(m^2·bar·h)]	B [L/(m^2·h)]	B_{Eq} [L/(m^2·h)]	B/B_{Eq}
Han et al. (2015) [38]	3.3	0.31	0.44	70%
Wan et al. (2015) [39]	3.4	0.28	0.48	58%
Zhang et al. (2015) [40]	3.5	0.31	0.53	58
Han et al. (2014) [41]	4.3	0.47	0.98	48.0%
Achilli et al. (2014) [42]	5.11	0.087	1.64	5.3%
Chou et al. (2012) [43]	3.32	0.14	0.45	31.1%

Therefore, a series of the PRO processes with different membranes and operating conditions are studied. It includes the ideal PRO process that has no CP or RSP, and the PRO process using different membranes. For ideal membranes, only water permeates across the membrane and the salts are fully rejected. And if the selectivity of the membrane can be improved with no loss on the water permeability, the performance of the scaled-up PRO process can be enhanced and shifts the economically viable PRO towards the larger specific membrane scale. As shown in Table 3, current membranes for PRO develop rapidly and the membrane permeability-selectivity has been improved. The relative salt permeability coefficients of the membranes, B/B_{Eq}, are reduced significantly. It demonstrates that the improvement on the membrane salt rejection can be done without the sacrifice of the water permeability. Therefore, in order to evaluate the potentials of the improved membranes, four virtual membranes are selected to represent the current and further improvement on the membrane. The virtual membranes have 0%, 10%, 30% and 50% of the relative solute permeability coefficient based on the trade-off permeability-selectivity relationship represented by equation (13). In other words, with the same water permeability of the membrane, the selectivity is improved at different levels for the four virtual membranes. In addition, two specific membrane scales, 0.05 $m^2/(L\cdot h^{-1})$ and 0.1 $m^2/(L\cdot h^{-1})$, are selected for the simulation. For convenience, only the performance of the co-current PRO process is illustrated. The results are shown in Fig. 5 in which several figures are shown with respect to the performance of the PRO process with different membranes and operating conditions. The SEE and APD are represented in colour-map and contour-line, respectively. The dimensionless flow rate is 0.5.

The results of ideal-PRO (I-PRO) modelling without the CP or RSP indicate the limiting performance of the SEE and APD in the two specific scale PRO processes to extract the energy from the mixing of seawater and wastewater. As shown in I-PRO modelling, the maximum SEE of the PRO process with specific membrane scale 0.1 $m^2/(L\cdot h^{-1})$ is slightly higher than that with the small scale 0.05 $m^2/(L\cdot h^{-1})$. In fact, the rapid reduction on the APD with the increase in the membrane scale is due to significantly reduced efficiency of the mass transfer. The maximum water flux occurs at the inlet and reduces rapidly along the membrane channel. As a result, the limiting maximum APD is significantly decreased when the scale of the PRO process increases. The limiting maximum APD is only 3.1821 W/m^2 in PRO of specific membrane area 0.1 $m^2/(L\cdot h^{-1})$. This means that the economic viability of power density can never be achieved in this configuration with the selected salinities.

Comparing the results of PRO process with different membrane solute permeability coefficients, the effect of the accumulated solute leakage on the different scale of the PRO can be evaluated. If there is no RSP in which membrane with zero solute permeability coefficient, the higher permeable membrane results in better performance of PRO process at a particular structural parameter. However, the CP effects cause significant reduction in the overall performance of the scaled-up PRO process. Especially in the PRO process using high permeable membrane, the maximum APD reduces rapidly with the increase in the structural parameter. Furthermore, compared to the remaining results shown in Fig. 5 when the RSP effect is considered, the overall performance of the scaled-up PRO process is found and the particular balanced membrane properties are identified. As shown in Fig. 5, with the increase on the membrane solute permeability coefficient, the optimum membrane properties move to the lower water permeability coefficients. Generally, a large solute permeability has two negative impacts on the performance: it reduces the peak water flux at the inlet and accelerates the solute leakage from the draw to the feed along the flow channel. In such a case, a low peak water flux occurs at the inlet and declines very fast due to the increasing feed

concentration. Thus, due to the rapidly reducing net driving force across the membrane, the water permeation is significantly decreased compared to the I-PRO and the accumulated leakage significantly reduce the net driving force compared to the results of the PRO with zero salt permeability coefficient. As a result, both the SEE and APD are reduced with the increase in the solute permeability. And the balanced membrane permeability-selectivity is moved

In fact, for a scaled-up PRO process, in order to meet the economically viable power density, a complex issue needs to be addressed. On one hand, for maximizing the SEE, the scale of PRO process should be increased to reach the maximum water permeation from the feed to the draw. On the other hand, the increasing scale significantly reduces the economic viability of the membrane. Thus an optimum specific membrane scale for PRO process is constrained for the economic viability. On the basis of the analysis on the improvement of the membrane selectivity, when the better membrane is used in PRO process, the larger scale of the process meeting the economic viability can be achieved. For example, as shown in Fig. 5, under the selected flow conditions and salinities, the maximum APD of the PRO with specific membrane scale 0.05 $m^2/(L\cdot h^{-1})$ is 5.2371, 4.8750 and 4.6847 W/m^2 for the three membranes with 10%, 30% and 50% of the solute permeability based on the trade-off relation represented by equation (13). It indicates that the economic viability of the PRO process using the membrane with 10% of the solute permeability can be achieved in the specific membrane scale 0.05 $m^2/(L\cdot h^{-1})$. In contrast, using another two membranes, the specific membrane scale needs to be further reduced to meet the economically viable power density. Therefore, the economic viability is an overall result of the specific membrane scale, membrane properties, and conditions of salinities and flows.

	Ideal PRO without CP or RSP	0% of solute permeability coefficient B	10% of solute permeability coefficient B	30% of solute permeability coefficient B	50% of solute permeability coefficient B
A_M^1	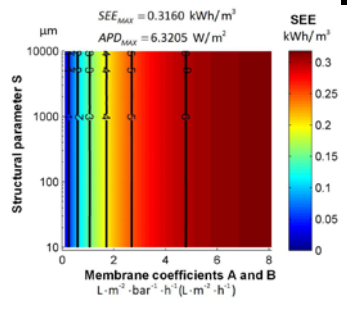	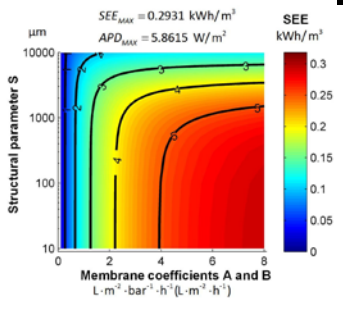	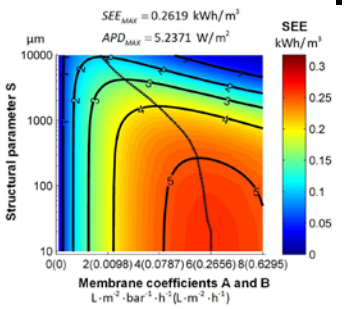	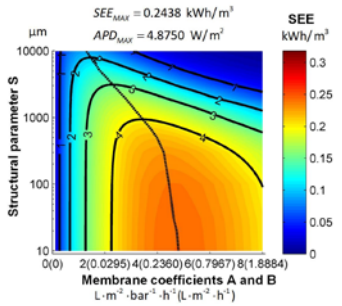	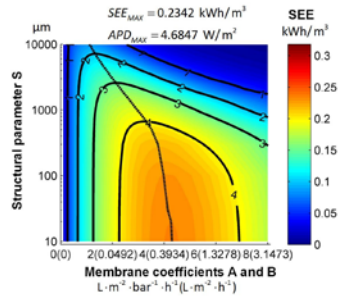
A_M^2	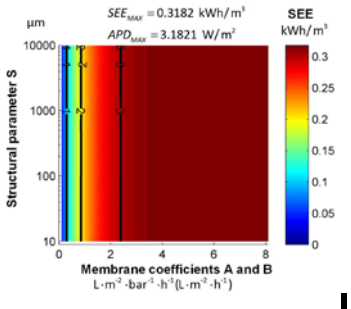	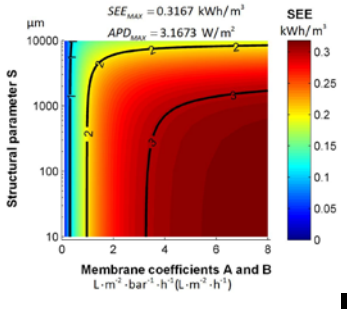	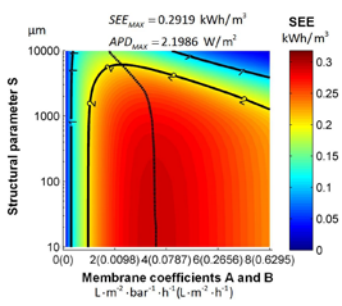	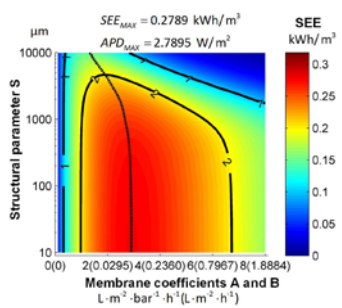	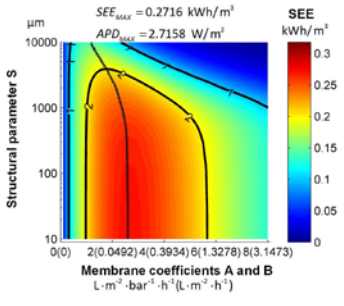

Fig. 5 Membrane sensitivity and process characteristics of co-current PRO. A_M^1 and A_M^2 are the selected specific membrane scales which are 0.05 and 0.1 , respectively.

5. Influence of process components efficiencies on the performance of the scaled-up PRO process

In the simulations of the scaled-up PRO process above, the performance is evaluated at the membrane module level, the inefficiencies of the process components are not considered. The HP, ERD and HT are all considered with 100% efficiency. However, in real applications, the energy losses in these components have a significant impact on the performance of the process. The efficiencies of the HP, ERD and HT are represented by η_{HP}, η_{ERD} and η_{HT}. Therefore, considering these machines' inefficiencies, the APD of a PRO process can be changed to

$$e_{C-PRO}^{Eff} = \frac{\Delta P_{PRO} \Delta V_P \eta_{HT} - V_D^0 \Delta P_{PRO} (1-\eta_{ERD}) / \eta_{HP}}{A_M} \tag{14}$$

For simplicity, with the negligible change on the density of the water during the PRO process, the ratio of the volumetric rates can be represented by the dimensionless flow rate, ϕ. Accordingly, the APD of the PRO process considering the inefficiencies can be further written as

$$e_{C-PRO}^{Eff} = e_{C-PRO}\eta_{HT} - \frac{(1-\phi)\Delta P_{PRO}(1-\eta_{ERD})\mathrm{V}_F^0}{A_M \phi \eta_{HP}} \tag{15}$$

where e_{C-PRO} is the APD of PRO with 100% efficiency components.

According to equation (15), it indicates the energy losses due to the inefficient machines can be divided into two main categories: energy loss in the salinity energy generation by HT which is considered by $e_{C-PRO}\eta_{HT}$, and energy loss in pressurizing the draw solution by ERD and HP which presented by the second part in equation (15).

Generally, the efficiency is dependent on the operating condition of the component. Efficiency of HP is highly a function of capacity, which depends on flow rate. The best efficiency can be achieved at the certain operational condition. For example, the choice of Ashkelon HPs brought the maximum possible pump efficiency 88.5% at its best point [44]. The best HT can be efficient hydraulically in the range of 80 to over 90%, and micro-hydro systems tend to be in the range of 60 to 80% efficient [45]. In addition, ERD available in the market mainly includes the Pelton Wheel, turbocharger, SWEER and Pressure Exchanger [46]. Compared to previous ERDs, such as Francis turbine, the efficiency of Pelton Wheel remains constantly high even during variations in the pressure and flow of feed, which is about 80 – 85% [47]. The hydraulic turbocharger is of the centrifugal type and has been in use since 1990s [48]. It consists of a HT and a HP. It is flexible in operation, easy to install and energy efficient compared with previous ERDs. The maximum efficiency achieved is 89-90% [48]. Different from the ERDs such as Pelton Wheel and turbocharger converting the hydraulic energy of brine to mechanical energy then to hydraulic energy, the DWEER and Piston pressure exchanger PX achieves the energy recovery by direct transfer of energy from hydraulic to hydraulic. As a result, the efficiency of PX is larger than 95%, up to 98% [49].

At the early stage for a preliminary analysis of the scale-up PRO process, for simplicity, constant efficiencies of the machines are assumed. Therefore, several sets of the possible efficiencies of the components are selected for further study, which are listed in Table 4 to represent the different components operated at the possible conditions (EFF1-EFF8) and an ideal condition (EFF9). The influence of the inefficiencies of the components is studied in the scaled-up PRO process in terms of

the APD considering different specific membrane area. In the simulation, due to the unchanged initial flow rate of the feed solution, the SEE can be estimated based on the APD and the specific membrane scale. Three dimensionless flow rates are selected for representing the low, medium and high dimensionless flow rates. The membrane properties are the same to the membrane used in Section 3. First the co-current flow scheme is considered.

TABLE 4 Selected sets of the components for the analysis of the machines' efficiencies.

Efficiency NO	**EFF1**	**EFF2**	**EFF3**	**EFF4**	**EFF5**	**EFF6**	**EFF7**	**EFF8**	**EFF9**
Efficiency of HP	70%	70%	70%	80%	90%	70%	70%	90%	100%
Efficiency of HT	80%	80%	80%	80%	80%	85%	90%	90%	100%
Efficiency of ERD	98%	95%	90%	90%	90%	90%	90%	98%	100%

The results are shown in Fig. 6 in which the nine sets of the machines are evaluated. The results clearly indicate that the hydraulic energy losses play a significant role in the PRO process. Theoretically, with the ideal machines (EFF9), because there is no energy loss of the pressurization, the maximum APD of a PRO process with a particular dimensionless flow rate should be achieved at the infinite small membrane area and is close to its peak power density as shown in Fig. 7(l). It is due to the maximum SEE achieved when a small amount of the feed solution mixed with the infinite draw solution in the level of the membrane module, namely at low dimensionless flow rate. As shown in Fig. 3, the maximum APD is located at the low dimensionless flow rate and low specific membrane scale. However, when the inefficiencies of the pressurization and expansion are considered in the system level, these hypothetical conclusions of the theoretical optimum cannot be realized in practice as illustrated in Fig. 6(a) – 6(h). For example, as shown in Fig. 6(h), although highly efficient machines are used, the APD characteristic of scale-up PRO process is significantly changed.

At a small membrane scale PRO process with a low dimensionless flow rate, the flow rate of the draw solution is relatively bigger than the flow rate of the feed solution. Although high APDs can be achieved in the membrane module level at a low dimensionless flow rate, it reduces significantly considering the energy losses in the pressuriation components in the system level. It is a result of the high flow rate of the draw solution being pumped and pressurized. Actually, at the small dimensionless flow rate, the energy loss during pumping and pressurizing the large volume of the draw solution overwhelms the salinity energy extracted from the permeation. Especially in the PRO at small specific membrane area, because of the limited salinity energy generated (limited SEE at the small specific membrane area as shown in Fig. 3), APD is significantly decreased. According to the results shown in Fig. 6(a) – 6(h), by using the set of components without 100% efficiencies, significantly reduced APDs are observed in all cases at the small specific membrane area. And with the increase on the inefficiency of the machines, the reductions of the specific membrane area are enlarged and the maximum of the APDs move to a large specific membrane area.

Furthermore, with the increase on the dimensionless flow rate, although APDs are reduced in the membrane module level, energy losses are also decreased due to the low flow rate of the draw

solution. As a result, the overall APD might be higher than that with a lower dimensionless flow rate. As shown in Fig. 6, the APDs of the PRO at the dimensionless flow rate 0.2 change significantly from (a) – (h) compared to those at the dimensionless flow rate 0.5 or 0.8. Due to the significantly decreased performance of the PRO at the low dimensionless flow rate, the PRO process with higher dimensionless flow rate, such as 0.5, shows better performance of the membrane in terms of APD at several studied cases. For example in Fig. 6(c), 6(d), 6(e), 6(f) and 6(g), the APDs of PRO with dimensionless flow rate 0.5 are larger than those with dimensionless flow rate 0.2. Thus, the optimum operation is shifted to a higher dimensionless flow rate. Furthermore, comparing the APDs of the PRO at dimensionless flow rate 0.5 and 0.8, it is found that the maximum APDs of the two operating conditions are similar in the study cases as shown in Fig. 6(a) – 6(h) but the optimum specific membrane areas are smaller for the scaled-up PRO with the dimensionless flow rate 0.8.

In addition, comparing the three machines considered, HT, HP and ERD, the efficiency of ERD is more sensitive to the performance of the PRO process. It is due to the fact that the pressurization of the initial draw solution is mainly done by the ERD by recycling the hydraulic energy of the brine and only the extra energy consumed by HP to cover the energy loss in the recycling due to the inefficiency of ERD. As shown in Fig. 6(a), 6(b) and 6(c), with the efficiency of ERD reduced from 98% to 95% and 90%, significant reductions of APD are found in all three operating conditions. However, according to the results of different HPs which are shown in Fig. 6(c), 6(d) and 6(e) and the results of different HTs which are shown in 6(c), 6(f) and 6(g), changes on the APD is less obvious.

Results shown in Fig. 6 are based on co-current flow scheme. Comparison between the two flows schemes are shown in Fig. 7 in which two sets of efficiencies are selected. The results show the increasingly preferred performance of the counter-current flow scheme when the specific membrane area increases. It is a result of the enhanced performance of the counter-current flow as shown in Fig. 3 to increase the salinity energy generation in the first part of equation (15).

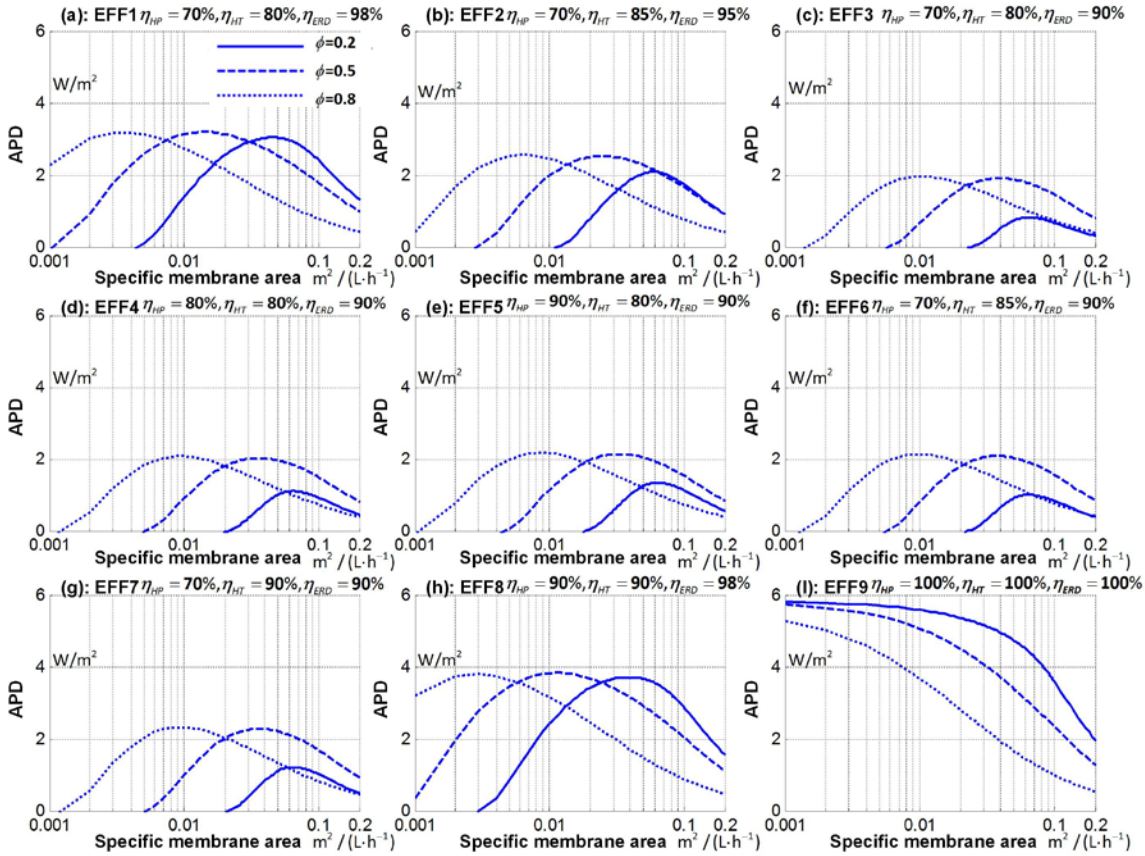

Fig. 6. influence of the inefficiencies of the HP, ERD and HT on the scaled-up PRO process.

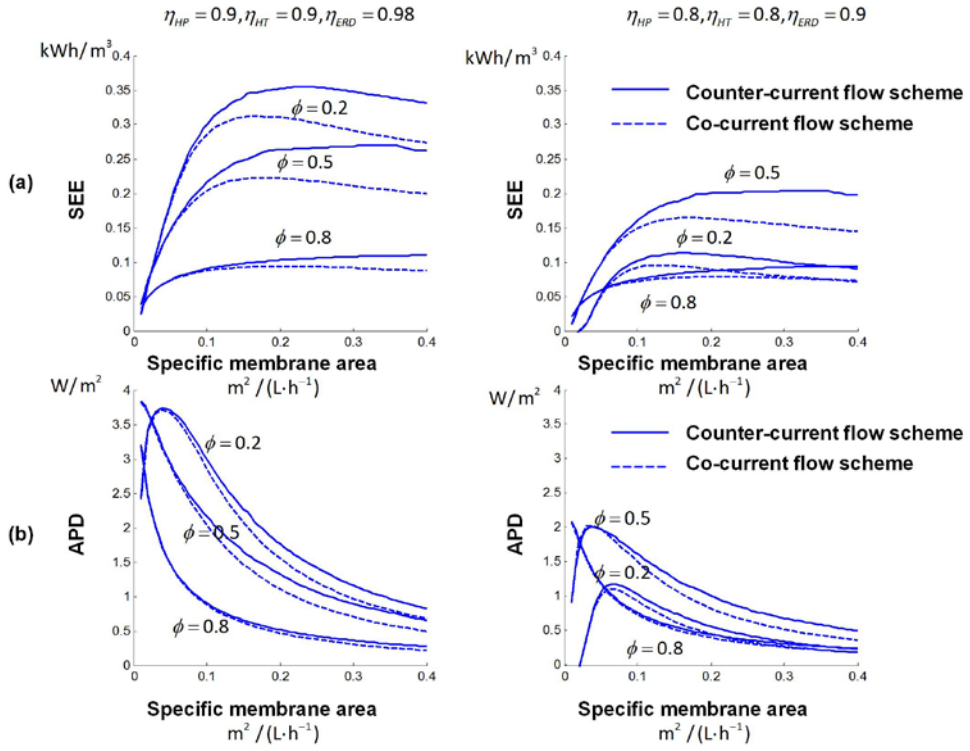

Fig. 7 Comparison between the co-current and the counter-current flow scheme.

6. Conclusion

A systematic evaluation and comparison between the co-current and the counter-current scaled-up PRO process is developed in this study. The significant operating conditions and design parameters of a scaled-up PRO process are investigated. It includes the hydraulic pressure applied on the draw solution, the initial flow rates of the draw and the feed solution, the permeability and selectivity of the membrane, structural parameter, and the inefficiencies of the process components such as HP, ERD and HT. On the basis of the results, some conclusions can be drawn: 1) dimensionless flow rate has an important role in the performance of the scaled-up PRO process in terms of both the SEE and the APD in the membrane module level. At a particular dimensionless flow rate, the process performance between the co-current and the counter-current flow scheme is not significantly different in high APD operations; 2) In the scaled-up PRO process, with the increase on the specific membrane scale, the detrimental effect of the RSP becomes significant. The accumulated solute leakage shifts the maximum SEE occurring at the lower membrane permeability in a larger scale PRO process. The ability to increase the SEE by enhancing the membrane permeability is better in the case of the counter-current flow PRO process.; 3) The machines' inefficiencies drive the maximum APD occurring at a higher dimensionless flow rate to reduce the energy losses in pumping and pressurization and a higher specific membrane scale to increase the salinity energy generation. The energy losses caused by the inefficiencies shrunk the salinity energy generation, especially at the small dimensionless flow in a small scale process.

Nomenclature

A	Membrane water permeability coefficient, $L \cdot m^{-2} \cdot h^{-1} \cdot bar^{-1}$
A_M	Membrane area, m^2
B	Membrane salt permeability coefficient, $L \cdot m^{-2} \cdot h^{-1}$
B_{Eq}	Paired membrane salt permeability coefficient based on Eq. (13), $L \cdot m^{-2} \cdot h^{-1}$
c_D	Concentration of solute in bulk of draw solution, $g \cdot kg^{-1}$
$c_{D,m}$	Concentration of solute at surface of membrane in draw solution, $g \cdot kg^{-1}$
c_F	Concentration of solute in bulk of feed solution, $g \cdot kg^{-1}$
$c_{F,m}$	Concentration of solute at surface of membrane in feed solution, $g \cdot kg^{-1}$
C_{OS}	Modified van't Hoff coefficient, $bar \cdot kg \cdot g^{-1}$
D	Bulk diffusion coefficient, $m^2 \cdot s^{-1}$
e	Average power density, $W \cdot m^{-2}$

E_{C-PRO} Specific extractable energy, $kWh \cdot m^{-3}$

J_W Water flux, $L \cdot m^{-2} \cdot h^{-1}$

J_S Solute flux, $L \cdot m^{-2} \cdot h^{-1}$

k Mass transfer coefficient, $L \cdot m^{-2} \cdot h^{-1}$

L Thickness of the active layer, m

m_S Solute permeation, $kg \cdot h^{-1}$

M_W Molar mass of water, $g \cdot mol^{-1}$

R_g Gas constant, $J \cdot K^{-1} \cdot mol^{-1}$

S Structural parameter, m

t_s Thickness of the porous layer, m

V_F^0 Initial volumetric flow rate of feed solution, $L \cdot h^{-1}$

W Power density, $W \cdot m^{-2}$

Greek symbols

ΔP_{PRO} Hydraulic pressure applied on draw solution, bar

Δq_P Mass flow rate of water permeation across the membrane, $kg \cdot h^{-1}$ ΔV_P Volumetric flow rate of water permeation across the membrane, $L \cdot h^{-1}$

ΔV_S Volumetric flow rate of RSP across the membrane, $L \cdot h^{-1}$

$\Delta \pi_m$ Osmotic pressure difference across the membrane, bar

δ Thickness of the boundary layer, m

τ Tortuosity of the support layer

ε Porosity of the support layer

ρ Density, $kg \cdot m^{-3}$

ϕ Dimensionless flow rate

β Fitting empirical parameter

λ Fitting empirical parameter, $cm^4 \cdot s^{-2}$

Subscripts and superscripts

0	Superscript denoting initial condition
$C-PRO$	Subscript denoting constant pressure PRO process
D	Subscript denoting draw solution
eff	Superscript denoting PRO process considering real machines
ERD	Subscript denoting energy recovery device
F	Subscript denoting feed solution
HP	Subscript denoting high pressure pump
HT	Subscript denoting hydro-turbine
P	Subscript denoting permeation

Reference:

[1] P. Bajpai, V. Dash, Hybrid renewable energy systems for power generation in stand-alone applications: A review, Renewable and Sustainable Energy Reviews, 16 (2012) 2926-2939.
[2] E. Trutnevyte, EXPANSE methodology for evaluating the economic potential of renewable energy from an energy mix perspective, Applied Energy, 111 (2013) 593-601.
[3] B. Shengrong, F.R. Yu, P.X. Liu, Z. Peng, Distributed Scheduling in Smart Grid Communications with Dynamic Power Demands and Intermittent Renewable Energy Resources, in: Communications Workshops (ICC), 2011 IEEE International Conference on, 2011, pp. 1-5.
[4] V.G. Gude, Energy storage for desalination processes powered by renewable energy and waste heat sources, Applied Energy, 137 (2015) 877-898.
[5] N.Y. Yip, M. Elimelech, Comparison of Energy Efficiency and Power Density in Pressure Retarded Osmosis and Reverse Electrodialysis, Environmental Science & Technology, (2014).
[6] S. Loeb, R.S. Norman, Osmotic Power Plants, Science, 189 (1975) 654-655.
[7] X. Li, T.-S. Chung, Thin-film composite P84 co-polyimide hollow fiber membranes for osmotic power generation, Applied Energy, 114 (2014) 600-610.
[8] W. He, Y. Wang, M.H. Shaheed, Enhanced energy generation and membrane performance by two-stage pressure retarded osmosis (PRO), Desalination, 359 (2015) 186-199.
[9] F. Helfer, C. Lemckert, Y.G. Anissimov, Osmotic power with Pressure Retarded Osmosis: Theory, performance and trends – A review, Journal of Membrane Science, 453 (2014) 337-358.
[10] K. Gerstandt, K.V. Peinemann, S.E. Skilhagen, T. Thorsen, T. Holt, Membrane processes in energy supply for an osmotic power plant, Desalination, 224 (2008) 64-70.
[11] N.Y. Yip, M. Elimelech, Performance Limiting Effects in Power Generation from Salinity Gradients by Pressure Retarded Osmosis, Environmental Science & Technology, 45 (2011) 10273-10282.
[12] N.Y. Yip, A. Tiraferri, W.A. Phillip, J.D. Schiffman, L.A. Hoover, Y.C. Kim, M. Elimelech, Thin-Film Composite Pressure Retarded Osmosis Membranes for Sustainable Power Generation from Salinity Gradients, Environmental Science & Technology, 45 (2011) 4360-4369.
[13] W. He, Y. Wang, M.H. Shaheed, Energy and thermodynamic analysis of power generation using a natural salinity gradient based pressure retarded osmosis process, Desalination, 350 (2014) 86-94.

[14] N.Y. Yip, M. Elimelech, Thermodynamic and Energy Efficiency Analysis of Power Generation from Natural Salinity Gradients by Pressure Retarded Osmosis, Environmental Science & Technology, 46 (2012) 5230-5239.
[15] S. Lin, A.P. Straub, M. Elimelech, Thermodynamic Limits of Extractable Energy by Pressure Retarded Osmosis, Energy & Environmental Science, (2014).
[16] A.P. Straub, S. Lin, M. Elimelech, Module-Scale Analysis of Pressure Retarded Osmosis: Performance Limitations and Implications for Full-Scale Operation, Environmental Science & Technology, (2014).
[17] L.D. Banchik, M.H. Sharqawy, J.H. Lienhard V, Effectiveness-mass transfer units (ε-MTU) model of a reverse osmosis membrane mass exchanger, Journal of Membrane Science, 458 (2014) 189-198.
[18] M.H. Sharqawy, L.D. Banchik, J.H. Lienhard V, Effectiveness–mass transfer units (ε–MTU) model of an ideal pressure retarded osmosis membrane mass exchanger, Journal of Membrane Science, 445 (2013) 211-219.
[19] L.D. Banchik, M.H. Sharqawy, J.H. Lienhard V, Limits of power production due to finite membrane area in pressure retarded osmosis, Journal of Membrane Science.
[20] M.F. Naguib, J. Maisonneuve, C.B. Laflamme, P. Pillay, Modeling pressure-retarded osmotic power in commercial length membranes, Renewable Energy, 76 (2015) 619-627.
[21] W. He, Y. Wang, M.H. Shaheed, Modelling of osmotic energy from natural salt gradients due to pressure retarded osmosis: Effects of detrimental factors and flow schemes, Journal of Membrane Science, 471 (2014) 247-257.
[22] J. Kim, M. Park, S.A. Snyder, J.H. Kim, Reverse osmosis (RO) and pressure retarded osmosis (PRO) hybrid processes: Model-based scenario study, Desalination, 322 (2013) 121-130.
[23] J.L. Prante, J.A. Ruskowitz, A.E. Childress, A. Achilli, RO-PRO desalination: An integrated low-energy approach to seawater desalination, Applied Energy, 120 (2014) 104-114.
[24] A. Achilli, J.L. Prante, N.T. Hancock, E.B. Maxwell, A.E. Childress, Experimental Results from RO-PRO: A Next Generation System for Low-Energy Desalination, Environmental Science & Technology, 48 (2014) 6437-6443.
[25] W. He, Y. Wang, M.H. Shaheed, Stand-alone seawater RO (reverse osmosis) desalination powered by PV (photovoltaic) and PRO (pressure retarded osmosis), Energy, 86 (2015) 423-435.
[26] B.J. Feinberg, G.Z. Ramon, E.M.V. Hoek, Scale-up characteristics of membrane-based salinity-gradient power production, Journal of Membrane Science, 476 (2015) 311-320.
[27] J.H. van't Hoff, The role of osmotic pressure in the analogy between solutions and gases, Journal of Membrane Science, 100 (1995) 39-44.
[28] D.E. Wiley, D.F. Fletcher, Techniques for computational fluid dynamics modelling of flow in membrane channels, Journal of Membrane Science, 211 (2003) 127-137.
[29] D.F. Fletcher, D.E. Wiley, A computational fluids dynamics study of buoyancy effects in reverse osmosis, Journal of Membrane Science, 245 (2004) 175-181.
[30] G.A. Fimbres-Weihs, D.E. Wiley, Numerical study of two-dimensional multi-layer spacer designs for minimum drag and maximum mass transfer, Journal of Membrane Science, 325 (2008) 809-822.
[31] A. Achilli, T.Y. Cath, A.E. Childress, Power generation with pressure retarded osmosis: An experimental and theoretical investigation, Journal of Membrane Science, 343 (2009) 42-52.
[32] B.D. Freeman, Basis of Permeability/Selectivity Tradeoff Relations in Polymeric Gas Separation Membranes, Macromolecules, 32 (1999) 375-380.
[33] A. Mehta, A.L. Zydney, Permeability and selectivity analysis for ultrafiltration membranes, Journal of Membrane Science, 249 (2005) 245-249.
[34] L.M. Robeson, Correlation of separation factor versus permeability for polymeric membranes, Journal of Membrane Science, 62 (1991) 165-185.
[35] R. Wang, L. Shi, C.Y. Tang, S. Chou, C. Qiu, A.G. Fane, Characterization of novel forward osmosis hollow fiber membranes, Journal of Membrane Science, 355 (2010) 158-167.

[36] A. Tiraferri, N.Y. Yip, W.A. Phillip, J.D. Schiffman, M. Elimelech, Relating performance of thin-film composite forward osmosis membranes to support layer formation and structure, Journal of Membrane Science, 367 (2011) 340-352.
[37] X. Song, Z. Liu, D.D. Sun, Nano Gives the Answer: Breaking the Bottleneck of Internal Concentration Polarization with a Nanofiber Composite Forward Osmosis Membrane for a High Water Production Rate, Advanced Materials, 23 (2011) 3256-3260.
[38] G. Han, J. Zuo, C. Wan, T.-S. Chung, Hybrid pressure retarded osmosis-membrane distillation (PRO-MD) process for osmotic power and clean water generation, Environmental Science: Water Research & Technology, 1 (2015) 507-515.
[39] C.F. Wan, T.-S. Chung, Osmotic power generation by pressure retarded osmosis using seawater brine as the draw solution and wastewater retentate as the feed, Journal of Membrane Science, 479 (2015) 148-158.
[40] S. Zhang, P. Sukitpaneenit, T.-S. Chung, Design of robust hollow fiber membranes with high power density for osmotic energy production, Chemical Engineering Journal, 241 (2014) 457-465.
[41] G. Han, Q. Ge, T.-S. Chung, Conceptual demonstration of novel closed-loop pressure retarded osmosis process for sustainable osmotic energy generation, Applied Energy, 132 (2014) 383-393.
[42] A. Achilli, J.L. Prante, N.T. Hancock, E.B. Maxwell, A. Childress, Experimental Results from RO-PRO: A Next Generation System for Low-Energy Desalination, Environmental Science & Technology, (2014).
[43] S. Chou, R. Wang, L. Shi, Q. She, C. Tang, A.G. Fane, Thin-film composite hollow fiber membranes for pressure retarded osmosis (PRO) process with high power density, Journal of Membrane Science, 389 (2012) 25-33.
[44] B. Sauvet-Goichon, Ashkelon desalination plant — A successful challenge, Desalination, 203 (2007) 75-81.
[45] O. Paish, Small hydro power: technology and current status, Renewable and Sustainable Energy Reviews, 6 (2002) 537-556.
[46] M.J. Guirguis, Energy Recovery Devices in Seawater Reverse Osmosis Desalination Plants with Emphasis on Efficiency and Economical Analysis of Isobaric versus Centrifugal Devices, in: Graduate School Theses and Dissertations, University of South Florida, 2011.
[47] M.B. Baig, A.A. Al Kutbi, Design features of a 20 migd SWRO desalination plant, Al Jubail, Saudi Arabia, Desalination, 118 (1998) 5-12.
[48] B. Peñate, L. García-Rodríguez, Energy optimisation of existing SWRO (seawater reverse osmosis) plants with ERT (energy recovery turbines): Technical and thermoeconomic assessment, Energy, 36 (2011) 613-626.
[49] C. Harris, Energy recovery for membrane desalination, Desalination, 125 (1999) 173-180.